

Copyright WILEY-VCH Verlag GmbH & Co. KGaA, 69469 Weinheim, Germany, 2013.

NANO MICRO  
**small**

Supporting Information

for *Small*, DOI: 10.1002/smll.201202878

**Decoupled Control of Carbon Nanotube Forest Density and Diameter by Continuous-Feed Convective Assembly of Catalyst Particles**

*Erik S. Polsen, Mostafa Bedewy, and A. John Hart\**

1 Supporting Information for DOI: 10.1002/sml.201202878

2

3 **Decoupled control of carbon nanotube forest density and diameter by continuous-feed**  
4 **convective assembly of catalyst particles**

5

6 By Erik S. Polsen, Mostafa Bedewy and A. John Hart\*

7

8 [\*] Prof. A. J. Hart, Erik Polsen, Mostafa Bedewy

9 Mechanosynthesis Group

10 Department of Mechanical Engineering

11 University of Michigan

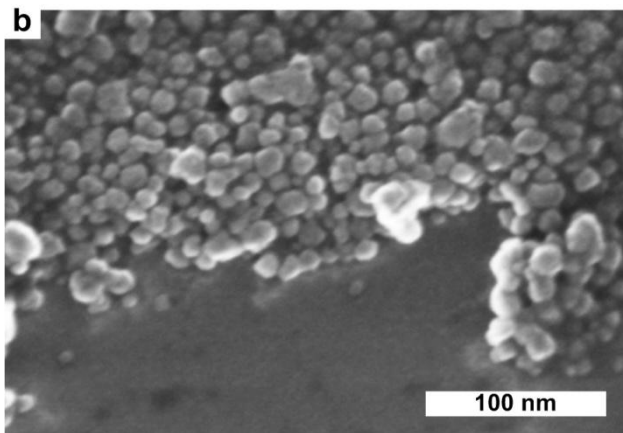
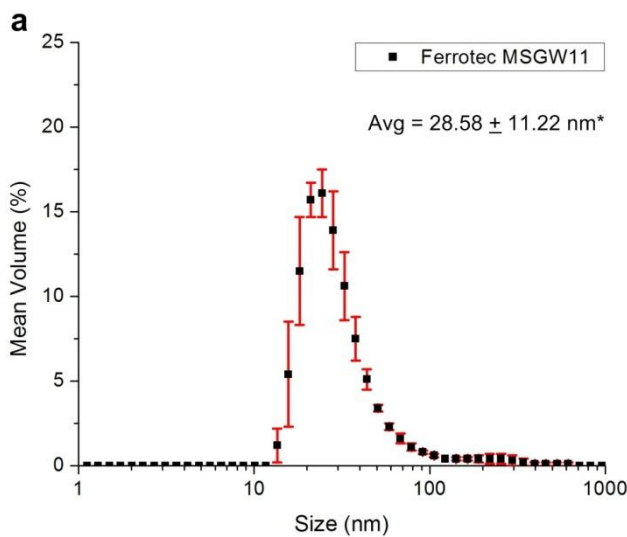
12 2350 Hayward Street

13 Ann Arbor, MI 48109 USA

14 E-mail: ajohnh@umich.edu

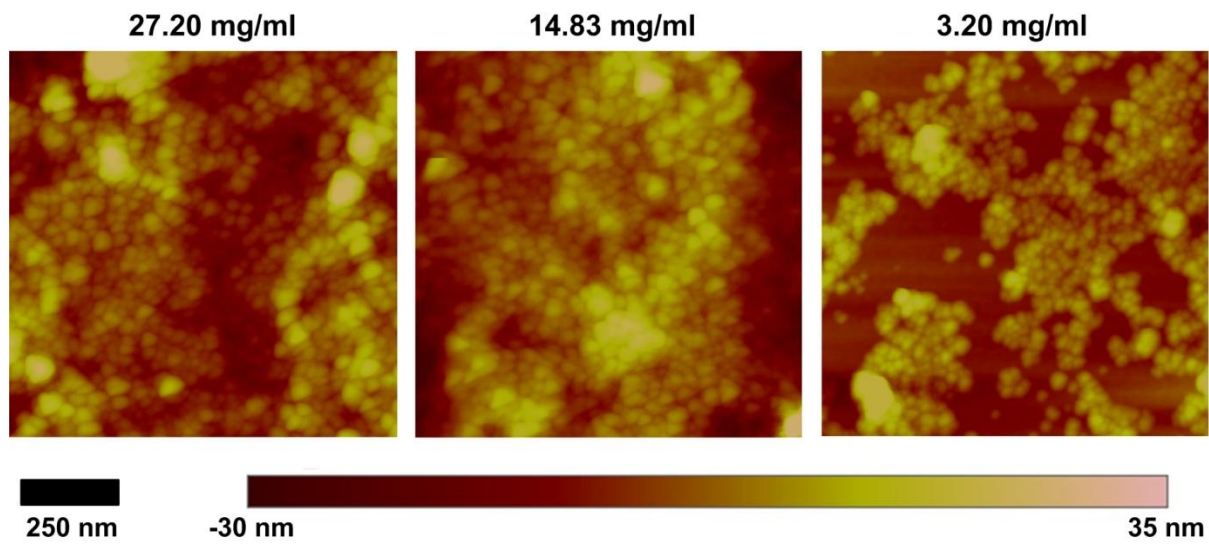
15

16



17

18 **Figure S1.** Particle size distribution and morphology for Ferrotec MSGW11 ferrofluid. a)  
19 DLS diameter distribution data from four separate measurements, and b) SEM of iron oxide  
20 particles from a 27.20 mg ml<sup>-1</sup> solution blade casted at 25 μm s<sup>-1</sup> on a substrate. \* Average  
21 diameter values are based on size data ≤ 70nm (which did not significantly impact the  
22 measurement, nor did the larger particles get deposited on the substrates during blade casting).

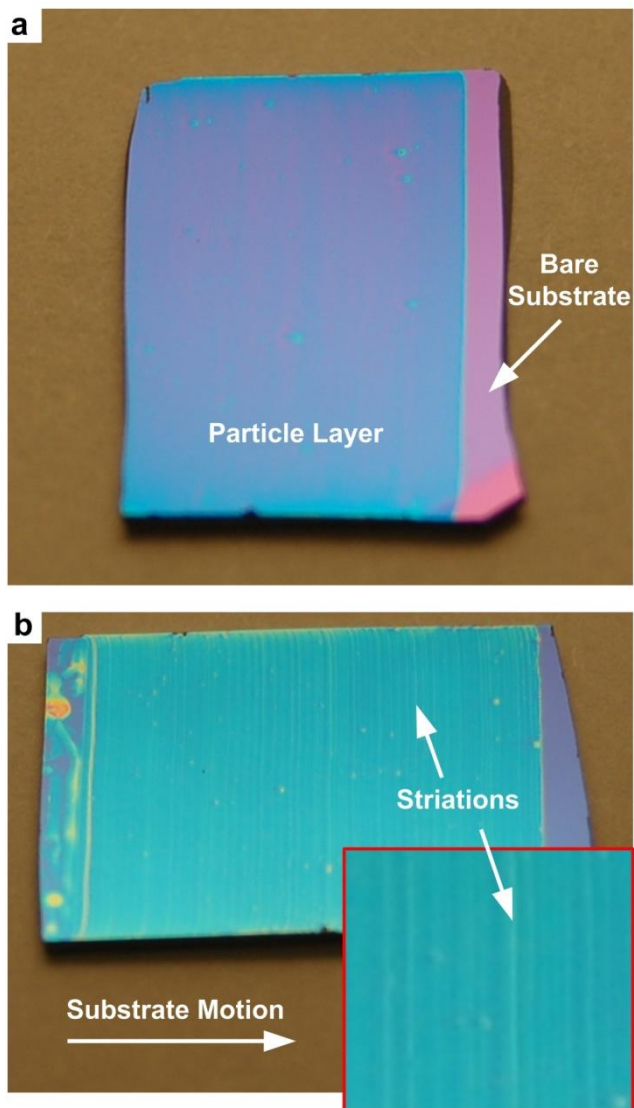


23

24

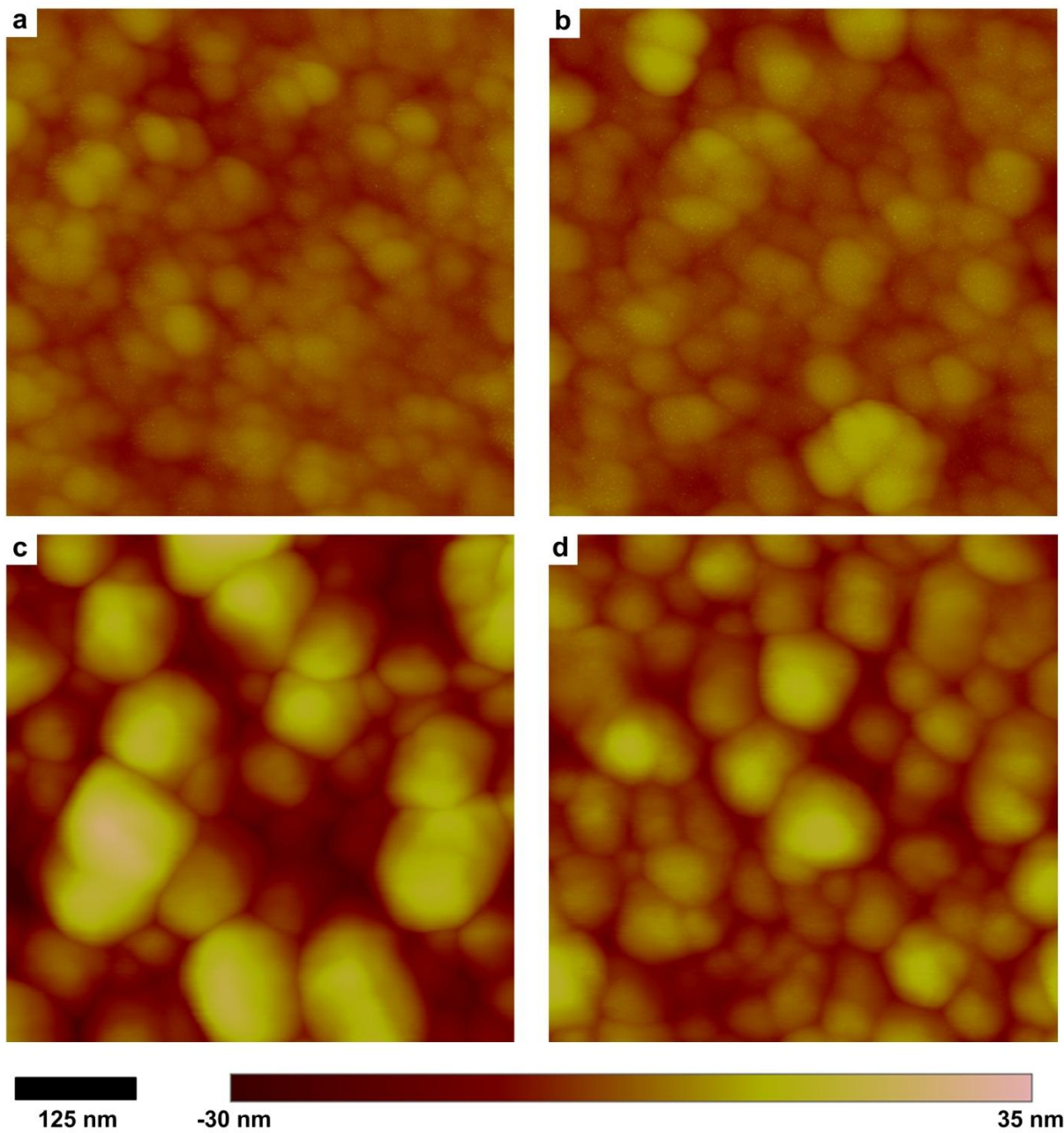
25

**Figure S2.** Iron oxide nanoparticle assembly using ferrofluid particle concentrations of 27.20, 14.83 and 3.20 mg ml<sup>-1</sup> on non-treated substrates at 25 μm s<sup>-1</sup>.



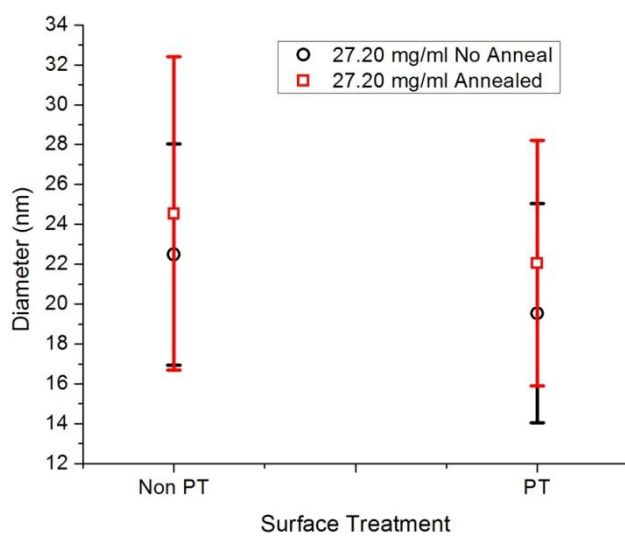
26

27 **Figure S3.** Optical particle layer uniformity as a result of blade casting parameters for  
28 Ferrotec MSGW11 ferrofluid. a)  $3.20 \text{ mg ml}^{-1}$  solution blade casted at  $50 \mu\text{m s}^{-1}$  b)  $27.20 \text{ mg}$   
29  $\text{ml}^{-1}$  solution blade casted at  $400 \mu\text{m s}^{-1}$  [inset: magnified image showing striations].



30

31 **Figure S4.** AFM comparison of pre and post annealed particles from a  $27.20 \text{ mg ml}^{-1}$   
32 ferrofluid solution blade casted at  $25 \mu\text{m s}^{-1}$  on both plasma-treated and non-treated substrates.  
33 (a) As-cast non-treated substrate, (b) As-cast plasma-treated substrate, (c) Annealed non-  
34 treated substrate, and (d) Annealed plasma-treated substrate.

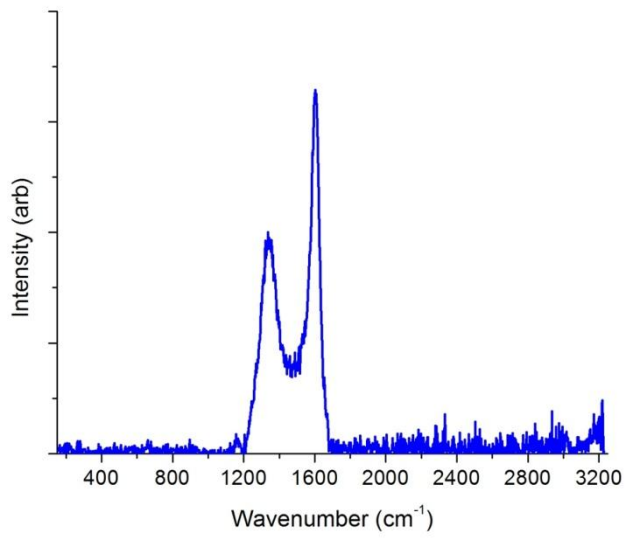


35

36

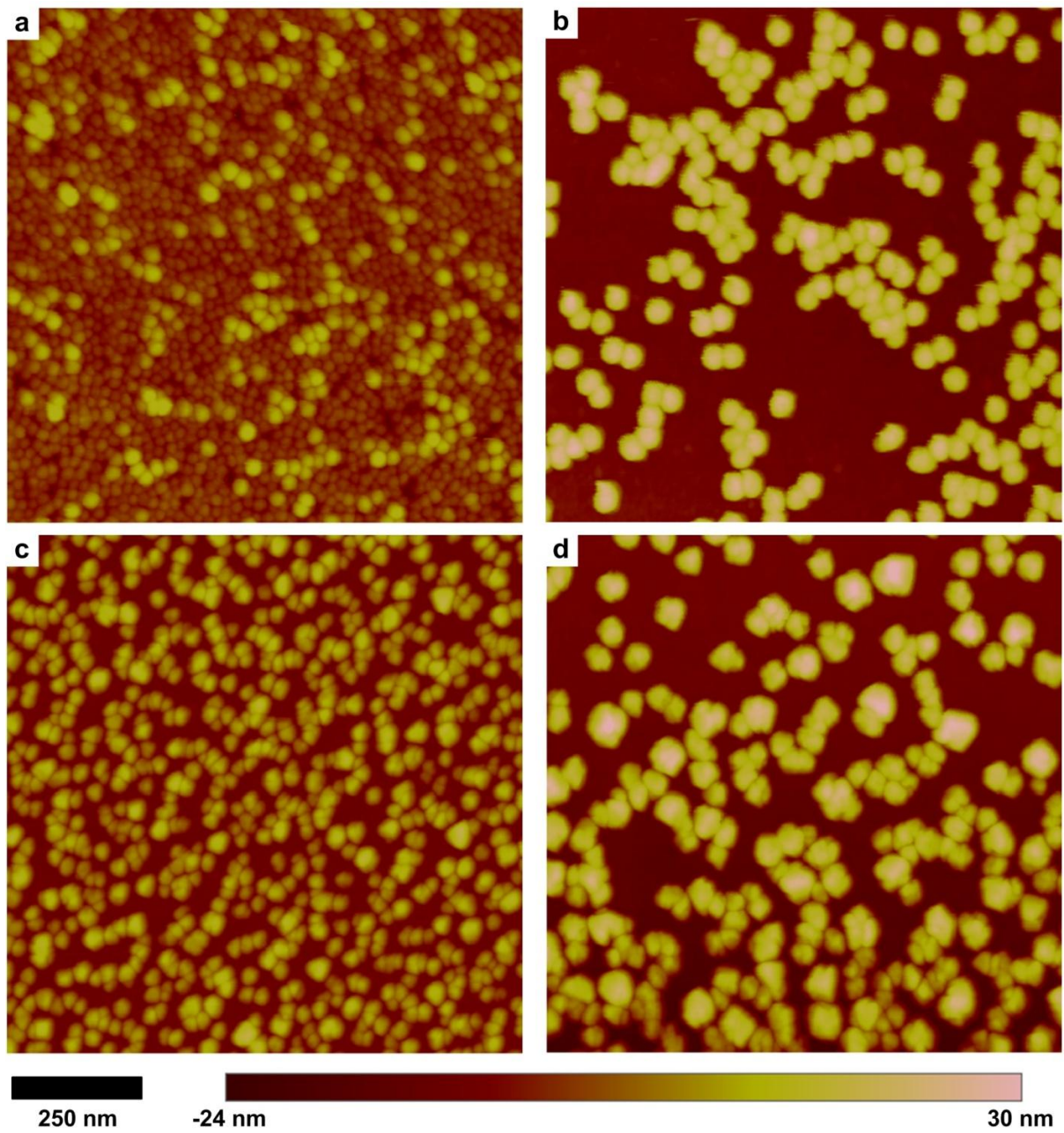
37

**Figure S5.** Analysis of iron oxide particle diameters pre and post annealing, on plasma-treated and non-treated substrates, blade casted from a 27.20 mg ml<sup>-1</sup> solution at 25 μm s<sup>-1</sup>.



38

39 **Figure S6.** Raman spectroscopy of carbon “flake” structure illustrating graphitic G and D  
40 peaks.



41

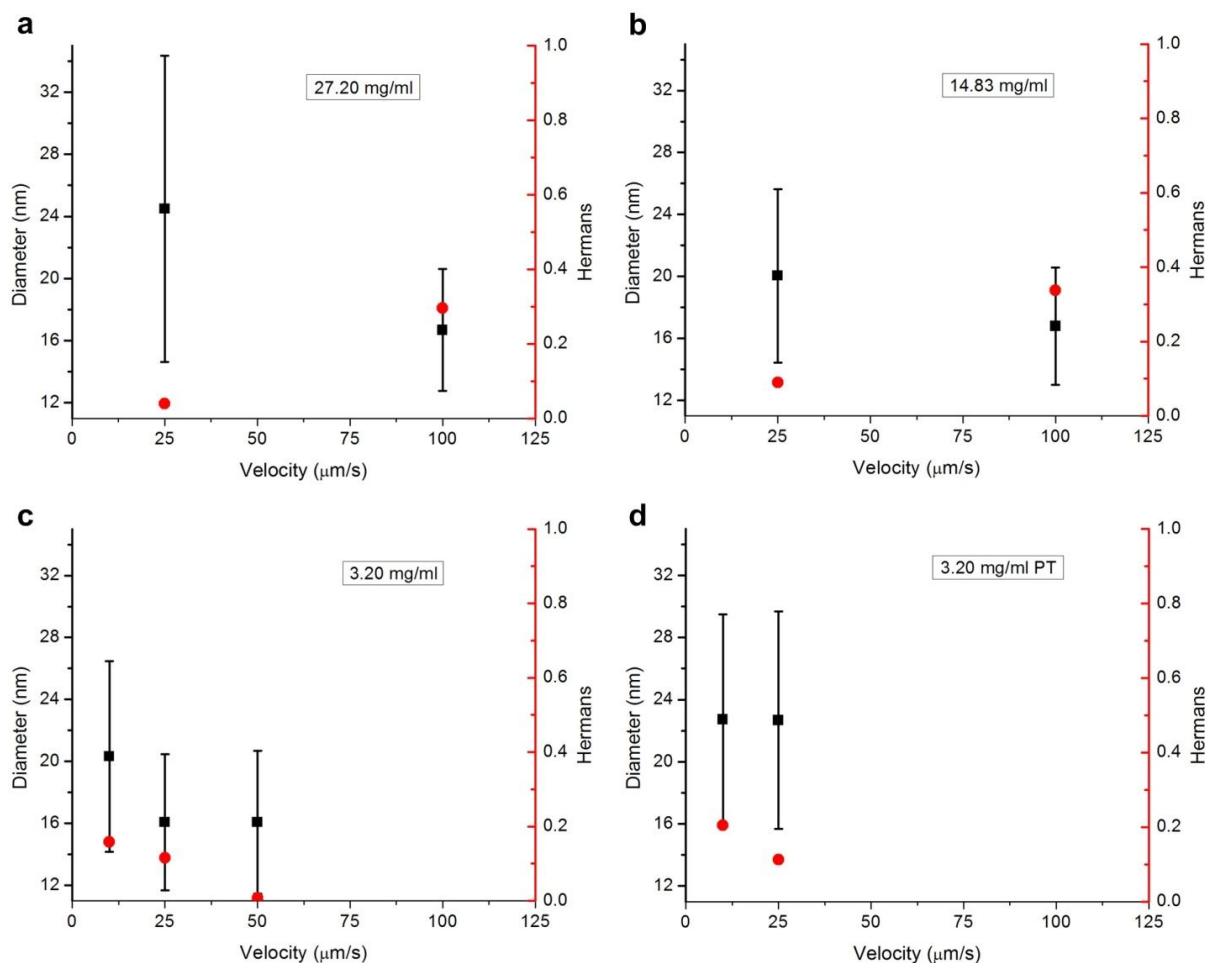
42

43

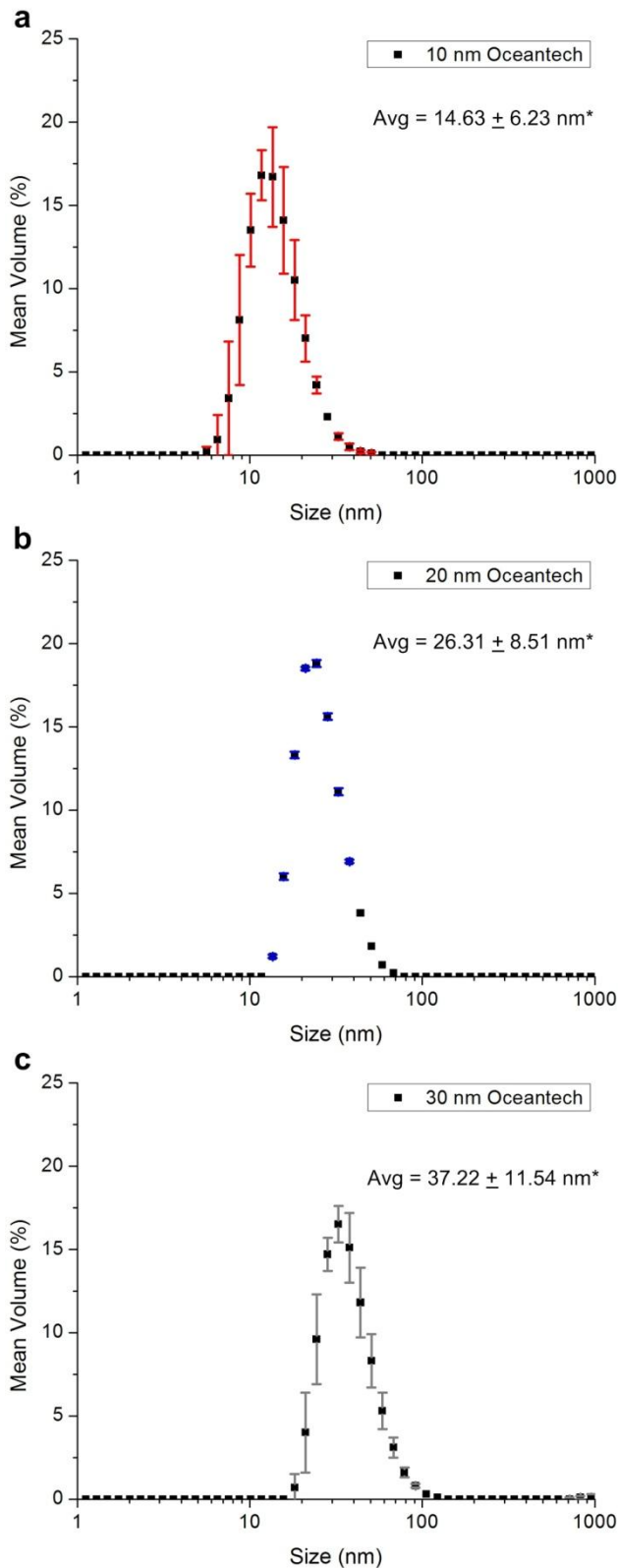
44

**Figure S7.** Coarsening of annealed particles from  $3.20 \text{ mg ml}^{-1}$  ferrofluid solutions blade casted at  $25 \mu\text{m s}^{-1}$ . (a) As-cast 20 nm particles, (b) As-cast 30 nm particles, (c) Annealed 20 nm particles, and (d) Annealed 30 nm particles.

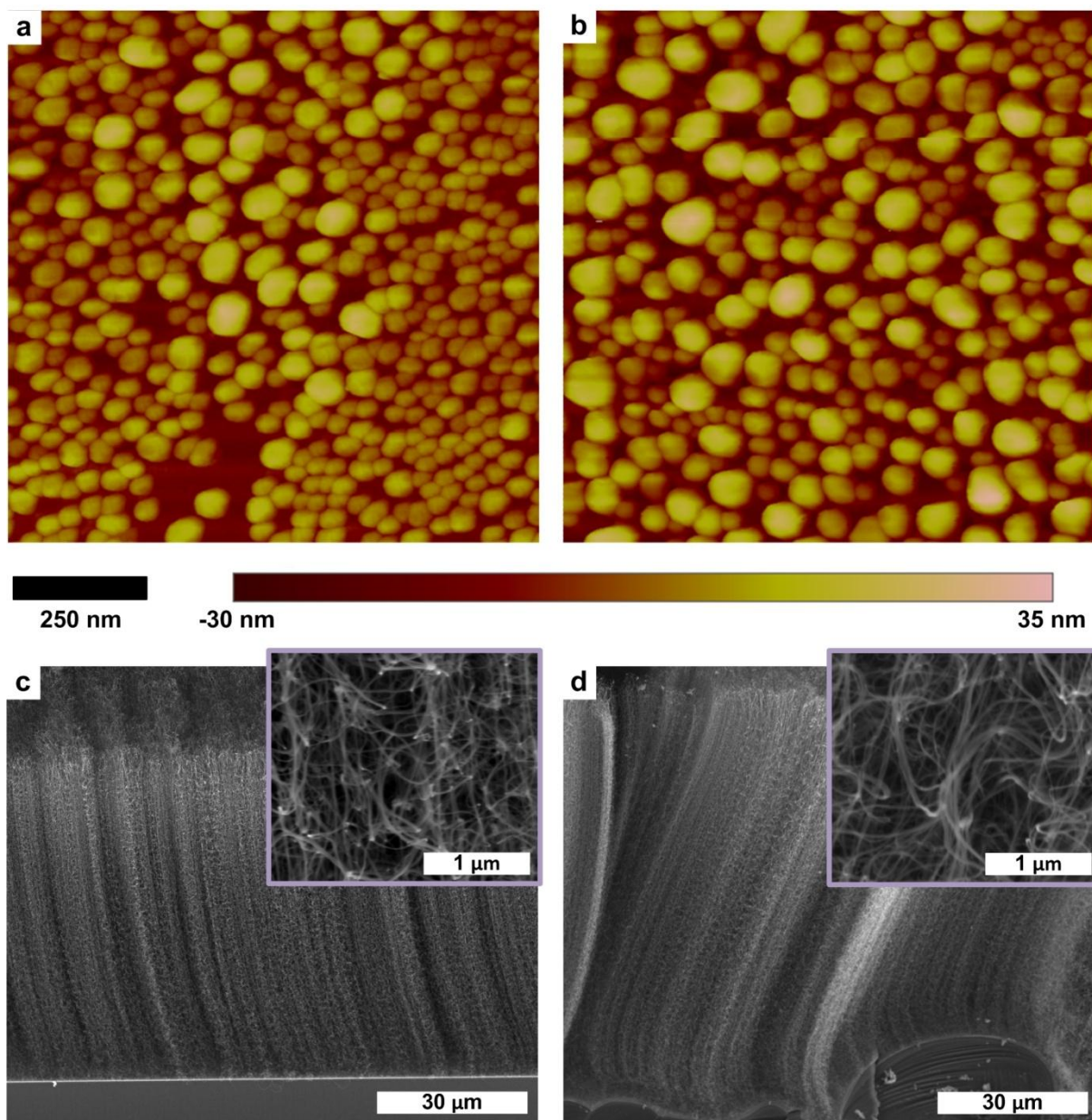




45  
46 **Figure S8.** SAXS analysis of VACNT arrays grown with MSGW11 ferrofluid solutions of  
47 varying concentrations. (a) CNT diameters and Hermans parameter for vertical alignment of  
48 grown arrays from a 27.20 mg ml<sup>-1</sup> solution, (b) CNT diameters and Hermans parameter for  
49 vertical alignment of grown arrays from a 14.83 mg ml<sup>-1</sup> solution, (c) CNT diameters and  
50 Hermans parameter for vertical alignment of grown arrays from a 3.20 mg ml<sup>-1</sup> solution, and  
51 (d) CNT diameters and Hermans parameter for vertical alignment of grown arrays from a 3.20  
52 mg ml<sup>-1</sup> solution blade casted on plasma-treated substrates.



53  
54 **Figure S9.** Particle size distributions and morphology for monodisperse Oceantech ferrofluid  
55 samples. Averaged DLS data for three runs per sample of (a) 10 nm iron oxide particles, (b)  
56 20 nm iron oxide particles, and (c) 30 nm iron oxide particles. \* Average diameter values are  
57 based on size data  $\leq 70$ nm (which did not significantly impact the measurement, nor did the  
58 larger particles get deposited on the substrates during blade casting).



59  
60 **Figure S10.** High-density monolayer of catalyst particles and corresponding CNT forest  
61 growth from the 30 nm nominal diameter particle solution (Fig. S9c). AFM images from  
62 annealed, blade-casted samples of (a)  $3.20 \text{ mg ml}^{-1}$  at  $10 \text{ } \mu\text{m s}^{-1}$ , and (b)  $12.0 \text{ mg ml}^{-1}$  at  $25$   
63  $\text{ } \mu\text{m s}^{-1}$ . SEM images of CNT forest growth (c) and (d), from samples (a) and (b) respectively.

64 **GOVERNING PRINCIPLES OF CONVECTIVE ASSEMBLY**

65

66 The linear growth rate ( $v_c$ ) of a particle monolayer, or multilayer, undergoing convective  
67 assembly is equal to:<sup>[1]</sup>

$$68 \quad v_c = \frac{\beta l j_e \varphi}{h(1-\varepsilon)(1-\varphi)}, \quad (1)$$

69 where  $\beta$  is a coefficient of proportionality,  $j_e$  is the volumetric evaporation flux per unit area  
70 of the solvent,  $l$  is the evaporation length (see Supporting Information),  $\varphi$  is the particle  
71 volume fraction in the suspension,  $h$  is the thickness of the layer, and  $\varepsilon$  is the porosity of the  
72 array. In order to maintain a steady growth rate of a particle monolayer according to Equation  
73 1, the relative motion speed between the blade and the substrate ( $v_r$ ) must equal  $v_c$ . If  $v_r > v_c$ ,  
74 a non-close-packed particle layer will be formed, whereas if  $v_r < v_c$ , multiple particle layers  
75 will be formed.

76 The coefficient of proportionality is defined as the ratio between the macroscopic mean  
77 velocity of the suspended particles ( $v_p$ ) and that of the solvent molecules ( $v_s$ ).

$$78 \quad \beta = v_p/v_s \quad (2)$$

79 Stronger particle-particle interactions and particle-substrate interactions decrease the value  
80 of  $\beta$ , whereas non-adsorbing particles and dilute solutions increase  $\beta$  close to a value of 1.

81 The evaporation length,  $l$ , is the ratio between the evaporation flux per unit length at the  
82 leading edge ( $J_{evap}$ ) and  $j_e$ .

$$83 \quad l = J_{evap}/j_e \quad (3)$$

84 Both  $J_{evap}$  and  $j_e$  are dependent on the local surrounding conditions illustrated by the  
85 Langmuir equation:

$$86 \quad \frac{dM}{dt} = (p_v - p_p) \sqrt{\frac{m}{2\pi RT}} \quad (4)$$

87 where  $p_v$  is the vapor pressure of the solvent,  $p_p$  is the partial pressure of the solvent in the  
 88 local atmosphere,  $m$  is the mass of a single solvent molecule,  $R$  is the ideal gas constant and  $T$   
 89 is the temperature. Dividing the Langmuir equation by the density of the solvent yields  $j_e$ .

$$90 \quad j_e = \left(\frac{dM}{dt}\right)/\rho \quad (5)$$

91 As temperature increases,  $p_v$  increases, increasing the evaporation flux based on the  
 92 Clausius-Clapeyron relation and results in an increased evaporation flux. Additionally,  
 93 increases in the relative humidity of the surrounding air limits the rate at which the solvent  
 94 molecules can be incorporated into the local atmosphere, which also increases  $p_p$  if the solvent  
 95 is water. The use of Equation 2 has been shown to be valid for particles with diameters down  
 96 to 79 nm, however, the mechanism of assembly with smaller particles still applies. While  
 97 functionalized particles on the order of 6 - 11 nm have been shown to include island  
 98 formation at the air-liquid interface prior to being pinned to the substrate,<sup>[2,3]</sup> the non-  
 99 functionalized particles used in this study did not display the formation of islands at the air-  
 100 liquid interface.

101 **CALCULATION OF CNT NUMBER DENSITY**

102

103 From the SAXS data, the arithmetic mean of the lognormal distribution of CNT diameter  
104 ( $D_0$ ) within the forest, and the average wall thickness ( $t$ ) of the CNTs are used to calculate the  
105 number of walls ( $n$ ) for the multi-walled CNTs, assuming a wall spacing equal to the  
106 interplanar spacing of graphite (0.34 nm)

107 
$$n = \frac{D_0 - t}{0.34}, \quad (6)$$

108 where  $D_0$  and  $t$  are in nm. The total distance around the sum of the circumferences of each  
109 CNT wall is calculated next

110 
$$C = \sum_{x=0}^{n-1} \pi(D_0 - 0.68x) \quad (7)$$

111 The height of the CNT forest ( $h$ ) measured from SEM imagery, is then divided by the  
112 number of SAXS measurements collected over the forest height ( $s$ ) to obtain the height of a  
113 single slice of the forest

114 
$$\Delta h = \frac{h}{s} \quad (8)$$

115 Taking CNT tortuosity into account, the average length of the CNTs ( $L$ ) are calculated  
116 using  $\Delta h$  from Equation 8 and the Hermans orientation parameter ( $H$ ) that was obtained for  
117 each slice of the CNT forest via SAXS

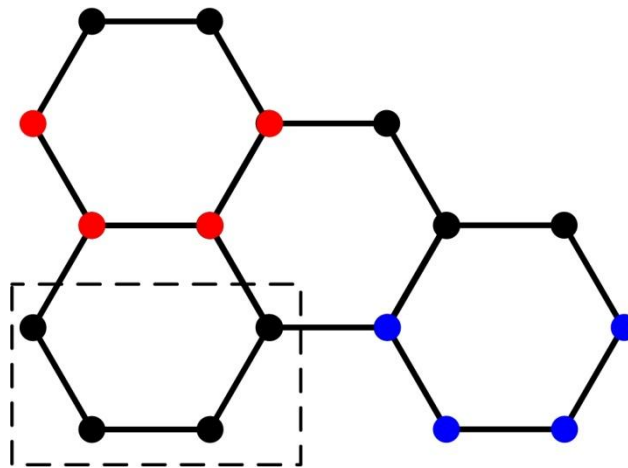
118 
$$L = \sum_{x=1}^s (\Delta h) \cos \left( \cos^{-1} \sqrt{\frac{2H_x + 1}{3}} \right) \quad (9)$$

119 Considering the hexagonal lattice of carbon atoms that make up the sidewall of CNTs, we  
120 can estimate the number of atoms in the average CNT within the forest. **Figure S11** shows a  
121 portion of a hexagonal lattice of carbon atoms where the unit cell is highlighted by the dotted

122 line. The separation between carbon atoms in this configuration is 0.142 nm, and so we can  
 123 calculate the spacing between unit cells in the x and y directions (shift to blue and red  
 124 positions respectively) as 0.426 and 0.246 nm respectively. With these dimensions we then  
 125 calculate the number of atoms ( $N$ ) for an average CNT (neglecting any cap) using the result  
 126 from Equation 9 in nm

$$127 \quad N = 4(L/0.246)(C/0.426) \quad (10)$$

128



129

130

**Figure S11.** Hexagonal lattice of carbon atoms.

131

132 Finally, we calculate the number of CNTs per unit area using  $h$ ,  $N$  and the measured  
 133 volumetric density of the forest ( $\rho$ )

$$134 \quad \text{CNTs / area} = \frac{\rho h N_A}{N(m_C)} \quad (11)$$

135 where  $N_A$  is Avogadro's Number and  $m_C$  is the atomic mass of carbon.

136 **References**

- 137 [1] A. S. Dimitrov, K. Nagayama, *Langmuir* **1996**, *12*(5), 1303–1311.
- 138 [2] T. P. Bigioni, X.-M. Lin, T. T. Nguyen, E. I. Corwin, T. A. Witten, H. M. Jaeger,  
139 *Nature Materials* **2006**, *5*(4), 265–270.
- 140 [3] M. I. Bodnarchuk, M. V Kovalenko, S. Pichler, G. Fritz-Popovski, G. Hesser, W.  
141 Heiss, *ACS nano* **2010**, *4*(1), 423–431.

142

143 Received: ((will be filled in by the editorial staff))

144 Revised: ((will be filled in by the editorial staff))

145 Published online on ((will be filled in by the editorial staff))